Extreme-Ultraviolet Light Source for Lithography Based on an Expanding Jet of Dense Xenon Plasma Supported by Microwaves

I. S. Abramov, E. D. Gospodchikov, and A. G. Shalashov[*]

Institute of Applied Physics of the Russian Academy of Sciences, 46 Ulyanova Street, Nizhny Novgorod 603950, Russia

We discuss a concept of a pointlike source of extreme-ultraviolet (EUV) light based on a nonequilibrium microwave discharge in an expanding jet of dense xenon plasma with multiply charged ions. The conversion efficiency of microwave radiation to EUV light is calculated, and physical constraints and possibilities for future devices are considered. Special attention is given to trapping of spontaneous line emission inside a radiating plasma spot that significantly influences the efficiency of an EUV light source.

I. INTRODUCTION

Transition to exposure using extreme-ultraviolet (EUV) radiation is vital for the development of next-generation projection lithography [1]. The only realistic method of EUV light generation is based on line radiation of multiply charged ions considering that stripping causes a shift of the ion emission spectrum toward shorter wavelengths for highly ionized charge states. In the EUV band, radiation is efficiently absorbed while propagating in the atmosphere and by elements of refractive optics [2]. Thus, EUV radiation should be manipulated in vacuum conditions and with reflective optics, such as multilayer mirrors. These mirrors have a narrow wavelength band where their reflection is high enough for efficient focusing of EUV radiation. Particular mirror materials and technology define the exact band of EUV radiation sources required by industry, and, consequently, the kind of emitting elements.

Most of the existing EUV sources operate at 13.5 nm $\pm$ 1%, corresponding to peak reflection coefficients of Mo/Si mirrors [3]. For this band, tin ions are an adequate choice due to a significant number of strong radiation lines at 13.5 nm $\pm$ 1% for Sn^{7+}–Sn^{12+}. The most-successful projects by ASML Cymer and Gigaphoton, which are almost ready for industry solutions, use evaporation of tin droplets in the focused beam of a CO_2 laser. The Gigaphoton source has an average EUV power above 100 W during 22 h of stable operation at 50 kHz and a conversion efficiency up to 5% [4]. The ASML machine [5] currently operates at 205 W, and developers are confident of achieving 250 W in 2018 [6]. That wattage saturates the current demand of microelectronics; however, the midterm development of lithography (a transition to less than 5-nm node) requires an EUV source of up to 1000 W, which,

experts believe, is nearly impossible to realize with a laser-produced plasma [6].

Another approach involving use of a microwave discharge, and that is potentially less constrained in terms of EUV power, is under development at the Institute of Applied Physics of the Russian Academy of Sciences. Microwave discharge has a number of other advantages over laser-produced plasmas, such as simpler overall design and safe operation for EUV collecting optics, which are saved from being spoiled by solid target particles and fast ions typical of explosive (of few nanoseconds) laser-produced plasmas. The duration of microwave pulses is longer [from tens of microseconds to continuous-wave (cw) operation], and there are no channels for significant ion heating due to direct resonant power load into electrons. In pioneer experiments, a strongly nonequilibrium tin plasma was confined in an open magnetic trap and heated by high-power microwaves, resulting in up to 50-W emission in the 13.5 nm $\pm$ 1% band [7–9].

Use of heavy noble gases, presumably xenon, instead of tin, opens new opportunities for microwave-based sources. Xenon ions are not as efficient emitters at 13.5 nm $\pm$ 1% as tin ions [10], but there is a whole family of strong lines in the 11.2 nm $\pm$ 1% band for Xe^{10+} and a few extra lines for neighboring ions [11–13]. For this band, there are Ru/Be and Mo/Be mirrors that have a nearly-twofold-higher peak reflection coefficient in 11.2 nm $\pm$ 1% in comparison with Mo/Si mirrors in the 13.5 nm $\pm$ 1% band [14]. Thus, a combination of xenon as the emitter and new mirrors operating at 11.2 nm $\pm$ 1% may potentially be more profitable for EUV lithography development.

The first successful experiments aimed at the realization of a pointlike highly emissive discharge in a noble gas have been reported [15–17]. Such experiments are possible with recent progress in a development of high-power gyrotrons operating at frequencies of 250–670 GHz and providing

a power of 100 kW and higher [18–20]. Going to higher frequencies allows a microwave discharge to be supported at higher plasma densities (more than 10^{16} cm^{-3} in the reported experiments), and thus increase in emissivity (up to 10 kW in the 110–180-nm band). In this case, the discharge may be ignited in a gas jet launched from a small nozzle at almost atmospheric pressure, and then it freely expands into a pumped-out chamber (7–200 mTorr at the wall).

In this paper, inspired by the success of recent experiments, we report a model predicting the conversion efficiency into the EUV band in the expanding gas jet and study the prospects of xenon-based EUV sources in present technological circumstances. An essential new feature of xenon discharge is the much higher plasma density (at least 2 orders of magnitude) than in tin plasma analyzed earlier [21–24]. Correspondingly, we consider new EUV emission physics taking into account the effects of radiation reabsorption in an optically thick plasma.

II. EUV SOURCE CONCEPT

The concept of an EUV light source with a freely expanding xenon plasma jet is illustrated in Fig. 1. Xenon is injected into a vacuum chamber with a nozzle, going through a paraboloid mirror used for collecting and focusing EUV light. High-power microwave radiation from a gyrotron is focused behind the nozzle and is resonantly absorbed by the electron component under conditions of plasma resonance when the electron Langmuir frequency becomes equal to the wave frequency. This condition is locally met somewhere along the expanding jet as electron density continuously decreases toward the collector. High electron thermal conductivity (typical for the plasma parameters considered) provides efficient heat transport outside the plasma resonance. Thus, the resonant heating may occur outside the EUV emitting zone (e.g., in a less-dense plasma), which allows the discharge to be supported over a wider range of microwave frequencies. Direct power load into electrons is beneficial for generation of highly charged ions. Such heating leads to high-electron-temperature nonequilibrium plasmas ($T_e \sim 100$ eV), while the ion temperature $T_i \lesssim 1$ eV, characterized by high rates of electron-impact ionization and line excitation and suppression of the recombination.

The setup operates in a quasistationary regime, which is more favorable to increase the efficiency of EUV emission. This is possible due to the long duration of microwave pulses for available gyrotrons (50 μs or longer) in comparison with the ion fly time through the chamber (a few microseconds). The most critical part of the discharge is related to its start-up, at which slow gas flow initially consisting of neutral species becomes ionized and accelerated up to ion-acoustic velocity [21–23]. Partial preionization of the flow would essentially decrease the average time that
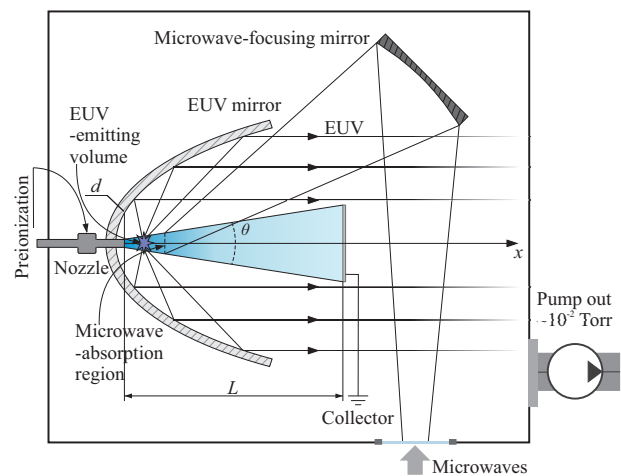

FIG. 1. Concept of EUV light source as proposed in Ref. [15].

an ion spends in low-charge stages and thus accelerates the transition to the stationary regime within the gyrotron pulse duration. Methods of such preionization are developed and checked experimentally.

Expanding plasma is absorbed by a metal collector located far from the emitting region. The decrease of plasma density with jet expansion provides good localization of the discharge, resulting, in particular, in the formation of a spotlike EUV emitting region near the nozzle (less than 1 mm in all dimensions for the reported experiments [15–17]). The latter allows efficient collection of EUV radiation.

III. THEORETICAL MODEL

Our model is based on the general description of a plasma flow with varying ion-charge composition due to step-by-step ionization [21–23]. The quasi-one-dimensional plasma flow with varying transverse cross section $\sigma(x)$ is described by ion-species densities $n_j(x)$, charge state $Z_j = j$ (e.g., charge je), and flow velocity $u(x)$. Assuming the electron temperature $T_e \sim 100$ eV (relevant to the experiment), one may ignore the electron-ion energy transfer due to elastic collisions and consider a strongly nonequilibrium plasma with $T_i \ll T_e$. This allows the ion pressure to be ignored in comparison with the electron pressure. At the same time, because of high electron heat conductivity $\chi_e \propto T_e^{5/2}$, one may ignore the electron-temperature variation within the emitting volume. Then, a stationary flow is described by the following set of fluid equations:

$$\frac{d}{dx}(\sigma n_j u) = \sigma(k_{j-1} n_e n_{j-1} - k_j n_e n_j), \quad n = \sum n_j,$$

$$\frac{d}{dx}(\sigma M n u^2) = -\sigma \frac{d}{dx}(n_e T_e), \quad n_e = \sum Z_j n_j,$$

representing the ionization balance and the total electron and ion momentum balance, respectively. Here M is the ion mass, n is the total density of ions, n_e is the electron density following from the quasineutrality condition, and $k_j(T_e)$ is the ionization coefficient of the jth ion.

Related to the EUV source, we need a continuous solution to the fluid equations in the vicinity of the ion-acoustic transition, which unavoidably follows from the flow expanding into a vacuum. In multicomponent plasmas, the finding of such a solution faces essential mathematical difficulties since the ion-sound velocity depends on the ion-charge distribution. Then, even location of the possible singularity along the flow is formally indefinite as it is governed by the preceding ionization dynamics. Nevertheless, this uncertainty may be overcome, and a *stable, stationary, continuous, and smooth* solution may be obtained if the fluid equations are solved with some very nontrivial boundary condition as proposed in Refs. [21,22]. Recently, this technique was applied and tested in a related study of an EUV light source based on a microwave discharge in a mirror magnetic trap [24].

Let the flow expand into the solid angle Ω starting from the nozzle with diameter d at $x = 0$. Then the cross section of the flow may be modeled as

$$\sigma(x) = \pi(d/2)^2 + \Omega x^2, \quad \Omega = 4\pi \sin^2(\vartheta/4),$$

where ϑ is the planar expansion angle (see Fig. 1). With the gas preionization in mind, we assume that plasma consists of singly ionized xenon at $x = 0$. Together with the conditions of the smooth ion-acoustic transition and the fixed gas puff rate $F = \sigma nu = $ const, this allows us to set the problem in a completed form.

The electron temperature enters the model as a parameter that may be defined from energy conservation. The power that is required to support the discharge at given T_e is equal to the the total power losses defined as

$$P = \left[\sigma nu \left(\frac{1}{2}Mu^2 + A\langle Z_j \rangle T_e \right) \right]_L + P_{\text{ion}} + P_{\text{exc}}. \quad (1)$$

The first term represents the convective losses corresponding to the kinetic energy flux to the collector located at $x = L$, $A = 1 + 0.5\ln(T_e/m_e u^2) \approx 3$ accounts for the ambipolar plasma potential [21], and $\langle Z_j \rangle = n_e/n$ is the average ion charge. The second term describes volumetric power losses for electron-impact ionization:

$$P_{\text{ion}} = \int_0^L p_{\text{ion}} \sigma \, dx, \quad p_{\text{ion}} = \sum_j E_j k_j n_e n_j,$$

where E_j is the ionization energy of the jth ion and p_{ion} is the power required to ionize a unit volume of multiply charged plasma per unit time. The third term describes power losses due to line excitation. Formally, this term may be represented in a similar way as the ionization losses:

$$P_{\text{exc}} = \int_0^L p_{\text{exc}} \sigma \, dx, \quad p_{\text{exc}} = \sum_j \sum_{h,l} \Delta E_{jhl} k_{jlh}^* n_e n_j, \quad (2)$$

where indices h and l numerate energy levels of the excited and ground electron configurations, respectively, for all allowed transitions in the spectrum of the jth ion, ΔE_{jhl} is the transition energy, k_{jlh}^* is the *effective* excitation coefficient, and p_{exc} is the *effective* power density.

In rarefied plasmas, once excited, an ion spontaneously relaxes to the ground state, emitting a photon, which freely escapes from the discharge volume; so, with good accuracy p_{exc} may be interpreted as an actual density of volumetric losses into solid angle 4π sr, and k_{jlh}^* is the usual excitation coefficient. This is exactly the case of the optically thin plasma considered in Refs. [21–24]. However, in the present paper we are considering plasma densities at least 2 orders of magnitude higher than before. The xenon jet tends to be in the opposite (optically thick) limit, at least for some spectral lines. In this case, we must take into account the possibility of radiation trapping inside the emitting volume, and then losses in a particular line may be attributed to emission from only an outer part of the discharge volume. This involves essentially new physics of radiation losses.

To calculate k_{jhl}^* corresponding to the arbitrary (optically dense or thin) plasma, we generalize a technique proposed by Holstein and Biberman [25] to account for multiple terms in the ground and excited electron configurations. The total power loss due to line excitation is expressed as

$$P_{\text{exc}} = \int \left(\sum_j \sum_{h,l} \Delta E_{jhl} A_{jhl} \theta_{jhl} \bar{n}_{jh} \right) dV, \quad (3)$$

where again h and l numerate terms of the excited and ground configurations, $\bar{n}_{jh}$ is the density of excited ions (we will use overbars and underlines to help distinguishing the lower and upper energy levels), A_{jhl} is the rate of spontaneous decay (the first Einstein coefficient), and θ_{jhl} is the probability of photon escape from the discharge volume. Under assumptions that the frequency of spontaneous emission quantum is distributed according to the line with shape $a(\omega)$ and the spatial distribution of emitting ions is uniform, one can determine the probability θ_{jhl} as the probability that a newly born photon will pass the characteristic linear dimension r_j of the volume occupied by jth emitting ion:

$$\theta_{jhl} = \int a(\omega) \exp[-r_j \kappa_{jhl}(\omega)] d\omega,$$

where κ_{jhl} is the absorption coefficient,

$$\kappa_{jhl}(\omega) = \frac{1}{4}(\bar{g}_{jh}/\underline{g}_{jl})\lambda_{jhl}^2 A_{jhl}\underline{n}_{jl} a(\omega),$$

$\bar{g}_{jh}$ and $\underline{g}_{jl}$ are statistical weights of the corresponding upper level and lower level in the $l \to h$ transition, $\underline{n}_{jl}$ is the population of the ground configuration of the jth ion corresponding to the lth energy level, and ω is the detuning from the line central frequency. The photon escape probability is strongly dependent on the mechanism of line broadening. In our case, the line form factor $a(\omega)$ must be calculated as a convolution of the Doppler and natural lines (the Voigt integral). In calculations we use approximate formulas for θ_{jhl} as a function of $r_j \kappa_{jhl}(0)$ developed by Apruzese [26] exactly for Voigt-broadened lines.

To define the density of excited ions, we consider the stationary equation of population balance for a *fixed upper energy level* under the assumption that only transitions from the ground configuration are possible (no further excitation of already excited states):

$$\frac{d\bar{n}_{jh}}{dt} = \sum_l [\underline{k}_{jlh} n_e \underline{n}_{jl} - (\bar{k}_{jhl} n_e + A_{jhl}\theta_{jhl})\bar{n}_{jh}] = 0, \quad (4)$$

where $\underline{k}_{jlh}$ and $\bar{k}_{jhl}$ are the electron-impact excitation and deexcitation coefficients for the $l \to h$ and $h \to l$ transitions, respectively, and $\underline{n}_{jl}$ and $\bar{n}_{jh}$ are the densities of the ground and excited configurations.

The rate of spontaneous decay is

$$A_{jhl} = \frac{2e^2}{m_e c^3}\left(\frac{\Delta E_{jhl}}{\hbar}\right)^2 \frac{\underline{g}_{jl}}{\bar{g}_{jh}} f_{jlh},$$

where f_{jlh} is the oscillator strength. The excitation coefficients, averaged over the Maxwellian electron distribution, may be estimated within the Bethe approximation for dipole-allowed transitions [27]:

$$\underline{k}_{jlh} = \frac{6e^4}{m_e^2 c^3}\left(\frac{2\pi m_e c^2}{3T_e}\right)^{3/2} \frac{\exp(-\varepsilon_{jhl})}{\varepsilon_{jhl}}\langle G(\varepsilon_{jhl})\rangle f_{jlh},$$

where $\langle G(\varepsilon_{jhl})\rangle$ denotes the thermally averaged Gaunt factor and $\varepsilon_{jhl} = \Delta E_{jhl}/T_e$. From the principle of detailed balancing, the deexcitation coefficient is

$$\bar{k}_{jhl} = \underline{k}_{jlh}(\underline{g}_{jl}/\bar{g}_{jh})\exp(\varepsilon_{jhl}).$$

Using the three equations above together, one can calculate the number of deexcitation acts per spontaneous decay transition as

$$\beta_{jhl} \equiv \frac{\bar{k}_{jhl} n_e}{A_{jhl}} = 3.7 \times 10^{-13}\frac{n_e(\text{cm}^{-3})}{T_e^{7/2}(\text{eV})}\frac{\langle G(\varepsilon_{jhl})\rangle}{\varepsilon_{jhl}^3}.$$

It is important to note that β_{jhl} does not depend on any line characteristic except the transition energy. Also, for the case studied, β_{jhl} is small compared with unity for the most-important lines.

The transition energy ΔE_{jhl} and the energy of free electrons are much higher than the difference between energy levels of the ground configuration; thus, the following condition is valid for any pair of levels l and l':

$$|\Delta E_{jhl} - \Delta E_{jhl'}| \ll \Delta E_{jhl}, \Delta E_{jhl'}, T_e. \quad (5)$$

Physically, it may be interpreted as lower levels are in contact with an effective thermal reservoir. Then the levels in the ground configuration are populated proportionally to the statistical weights:

$$\underline{n}_{jl} = \alpha_{jl} n_j, \quad \alpha_{jl} = \underline{g}_{jl}\left(\sum_{l'}\underline{g}_{jl'}\right)^{-1},$$

where n_j is the total density of unexcited jth ion, which is approximately equal to the total jth ion density. This allows us to solve Eq. (4) for the population of excited levels as

$$\bar{n}_{jh} = \frac{\sum_{l'}\alpha_{jl'}\underline{k}_{jl'h}}{\sum_{l'}A_{jhl'}(\theta_{jhl'} + \beta_{jhl'})}n_e n_j.$$

Substituting this solution into Eq. (3), we find the effective volume density of power loss is

$$\frac{dP_{\text{exc}}}{dV} = \sum_j \sum_{h,l}\frac{\Delta E_{jhl}A_{jhl}\theta_{jhl}\sum_{l'}\alpha_{jl'}\underline{k}_{jl'h}}{\sum_{l'}A_{jhl'}(\theta_{jhl'} + \beta_{jhl'})}n_e n_j. \quad (6)$$

When calculating the sum over the ground levels, one must keep in mind condition (5). From this condition, we have $\Delta E_{jhl} \approx \Delta E_{jhl'}$ and $\beta_{jhl} \approx \beta_{jhl'}$ (i.e., both quantities may be treated as independent of l). Then changing of the summation order over l and l' in Eq. (6) gives

$$\frac{dP_{\text{exc}}}{dV} = \sum_j \sum_{h,l}\alpha_{jhl}\eta_{jh}\Delta E_{jhl}\underline{k}_{jlh}n_e n_j, \quad (7)$$

with

$$\eta_{jh} = \frac{\sum_{l'}A_{jhl'}\theta_{jhl'}}{\sum_{l'}A_{jhl'}(\theta_{jhl'} + \beta_{jhl'})}. \quad (8)$$

After averaging over the jet cross section σ, we find these formulas result exactly in Eq. (2) with $k_{jhl}^* \equiv \alpha_{jhl}\eta_{jh}\underline{k}_{jlh}$.

Parameter η_{jh} has a clear physical interpretation: for each isolated transition $h \to l$ in Eq. (6), η_{jh} is the ratio of actual losses to possible radiative power losses if the trapping effect is ignored. Consequently, for optically thin lines, $\beta_{jhl} \ll \theta_{jhl}$, the trapping parameter η_{jh} is close to unity. In the opposite limiting case of optically thick lines, $\beta_{jhl} \gg \theta_{jhl}$, the trapping parameter vanishes: $\eta_{jh} \ll 1$. In other words, this parameter takes into account the effective decrease of the region contributing to losses of the (jh)

line; such volume is defined by the condition

$$\sum_l A_{jhl}\theta_{jhl}(\mathbf{r}) \gtrsim \sum_l A_{jhl}\beta_{jhl}.$$

Note that this condition is independent of l (i.e., transitions to different ground levels l corresponding to the same excited level h become trapped simultaneously).

In the following, we define the fraction of power emitted in the target EUV band. It may be characterized by the EUV conversion efficiency defined as

$$CE = P_{EUV}/P,$$

where P_{EUV} is calculated with Eq. (6), in which only transitions in the 11.2 nm ± 1% band are taken into account in the summation over (h, l), while the sum over l' is done over all allowed transitions. Alternatively, one may use Eq. (7) with η_{jhl} redefined such that only transitions in the EUV band are taken into account in the numerator of Eq. (8), while all other sums are calculated for all allowed transitions.

IV. ATOMIC DATA FOR XENON

The width of the considered EUV band of 11.2 nm ± 1% is comparable to the difference between terms in the ground and excited electronic states. Therefore, the complete structure of the electron configuration for xenon ions should be taken into account.

To calculate electron-impact excitation cross sections we use the Bethe approximation; thus, for the input, we need oscillator strengths, energy levels, and statistical weights. For 11.2 nm ± 1% lines, all data needed are taken from Refs. [11,12], essentially based on high-resolution spectral measurements in the deep-ultraviolet region for Xe^{9+} and Xe^{10+}. For all other lines, the spectral data are calculated with Cowan's code [28]. In the modeling, only allowed transitions are taken into account as they have much higher probabilities than the forbidden transitions, and the spectra contain a significant quantity of $\Delta n = 0$ resonance lines that correspond to a situation when the allowed transitions dominate.

In the absence of any information concerning the electron distribution function in the discharge, the cross sections are averaged over the Maxwellian velocity distribution. We use the averaged Gaunt factor as formulated by Van Regemorter [29] with the correction of Sampson and Zhang [30].

Features of Xe^+–Xe^{12+} spectral lines are illustrated in Fig. 2. Every line is characterized by its wavelength λ_{jhl}, oscillator strength f_{jlh}, and trapping parameter η_{jh} for a range of emitting-ion densities. The ion spectrum shifts toward the EUV region with increase of charge. For ion densities up to 10^{17} cm^{-3}, the plasma is almost optically thin for EUV radiation. At the same time, radiation of many strong lines with smaller transition energies (longer wavelengths) may be trapped in the discharge volume, which is beneficial for the conversion efficiency into the EUV band (near 10 nm). The optimal value of the ion
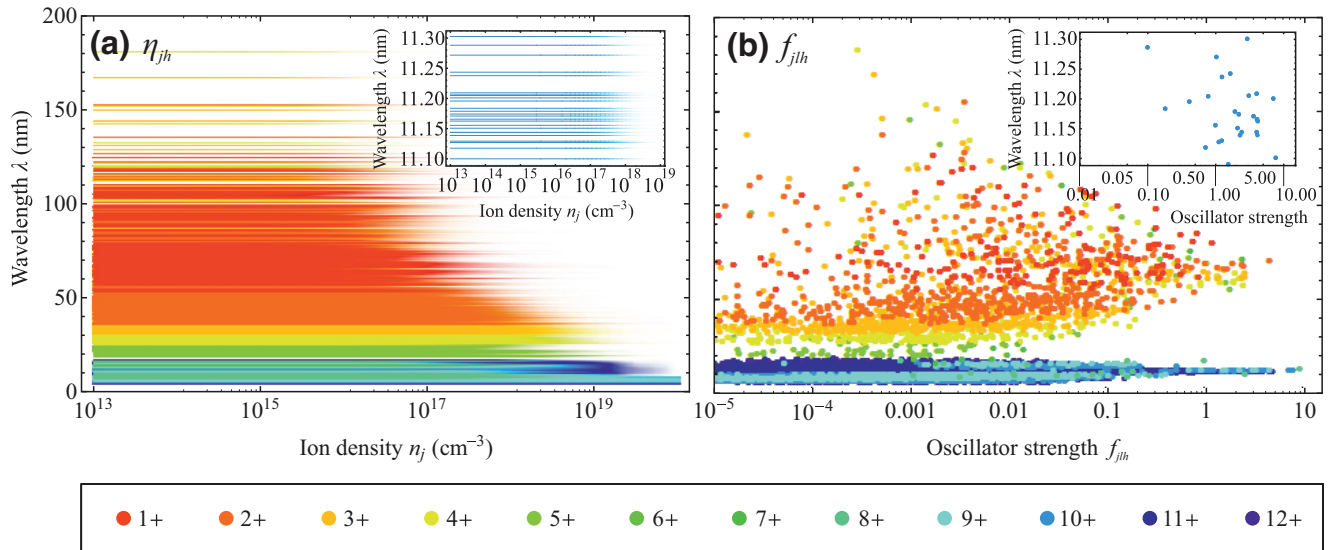

FIG. 2. (a) Dependence of the trapping parameter η_{jh} on the density n_j of the excited jth ion: the ordinate indicates the transition wavelength λ_{jhl}, different ion charges j are shown with different colors, with brightness proportional to the value of η_{jh}, maximum intensities correspond to optically thin lines with $\eta_{jh} \approx 1$, and vanishing colors correspond to trapped lines with $\eta_{jh} \ll 1$. (b) Oscillator strengths f_{jlh} corresponding to the same transition wavelengths. The inset shows Xe^{10+} lines in the 11.2 nm ± 1% band in more detail. The calculation parameters are $T_e = 50$ eV and $n_e = Z_j n_j$, and the characteristic linear dimension of the discharge is 100 μm.

density in the discharge for EUV light generation seems to be somewhere in between 10^{17} and 10^{18} cm^{-3}, where EUV (including 11.2 nm $\pm$ 1%) lines are almost the sole contributors to radiation loss. Densities above 10^{18} cm^{-3} are not expedient for EUV light generation, at least for the typical example of a discharge with characteristic dimensions of about 100 μm considered. A similar result was obtained independently for laser-produced plasma by Izawa *et al.* [31], who studied 13.5 nm $\pm$ 1% radiation sources based on tin-droplet evaporation. Thus, our conclusion on the upper limit for density, related to EUV light trapping, seems to be general.

Monoenergetic cross sections of electron-impact ionization are taken from Ref. [32], and then averaged over the Maxwellian electron distribution function.

V. CONSTRAINTS FOR EUV SOURCES BASED ON A DENSE-XENON-PLASMA JET

The model described is used to simulate the setup sketched in Fig. 1. The control parameters studied are as follows:

(a) The nozzle diameter d
(b) The gas puff rate, which is equal to the conserved total particle flux, $F = \sigma n u$
(c) The electron temperature T_e

In experiments, the gas puff rate is tuned by adjustment of the pressure at the nozzle output. Thus, to simplify a link to experiments, along with the gas puff rate we use the reference nozzle pressure $p = T_0 F/(\sigma_0 v_0)$ calculated under the assumption that a gas with room temperature $T_0 = 300$ K flows with sound velocity $v_0 = (\frac{5}{3}T_0/M)^{1/2}$ through the nozzle cross section $\sigma_0 = \pi d^2/4$ and providing the flux F. The electron temperature is controlled with the microwave power. Assuming that all microwave power is absorbed by electrons, the electron temperature may be treated just as a measure of the total power load into the discharge; that is, $P = P(T_e)$ is a known function given by Eq. (1) for the fixed nozzle diameter and gas puff rate.

Before we give the numerical results, it is worth describing the underlying physics. An efficient EUV light source must satisfy two conditions:

(a) The plasma consists of a significant number of Xe^{10+} ions since exactly these particular ions emit radiation in the 11.2 nm $\pm$ 1% EUV band.
(b) The emitting volume is optically thin (i.e., the plasma density and discharge dimensions are limited to avoid the radiation-trapping effect in the EUV band).

To meet these requirements, we vary F, T_e, and d.

An increase of the gas puff rate (by increase of the nozzle pressure) leads to increase of both electron average density and ion average density in the discharge. The higher the electron density, the more efficient is the electron-impact ionization and excitation, but the higher is the deexcitation rate. The increase of ion density results in more emitters and, at the same time, more absorbers of the line radiation (more efficient trapping). As a result of a neat balance between emission and absorption, there is an optimal value of the gas puff rate at which the conversion efficiency into EUV light is maximal.

The higher the gas puff rate is, the greater is the power required to support a particular electron temperature T_e. As the excitation and ionization rates strongly depend on the electron temperature, the microwave power defines whether the needed Xe^{10+} ions are born in the discharge or not, and determines the efficiency of their line radiation. But electron temperatures that are too high cause significant convective power losses as the flow velocity increases (which scales approximately as the ion-acoustic velocity $v_a = \sqrt{T_e \langle Z \rangle/M}$). At the same time, as the total flux $F = \sigma n u$ is conserved, the ion density decreases, resulting in decrease of the emissivity. A balance between these effects defines the optimal electron temperature or the optimal power load.

On the other hand, the nozzle diameter affects the optimal power and the optimal plasma flux, both increasing with the diameter. Thus, one may adjust these values for practical requirements by varying the nozzle diameter. Such adjustment of the nozzle diameter may be beneficial also for the optimization of EUV conversion efficiency. The convective power losses are proportional to d^2, while the volumetric power losses, presumably due to line emission for *optically thin* Xe^{10+} plasma, increase as d^3. So, the conversion efficiency tends to increase with the nozzle diameter until the plasma is optically thin for EUV light.

The above statements are illustrated in Fig. 3. Here the EUV conversion efficiency and EUV power are plotted as a function of the nozzle gas pressure (gas puff rate) and the electron temperature for a fixed nozzle diameter. One can see that there is a combination of the gas pressure and microwave power providing the maximum conversion efficiency (marked with a star). At this point, the total power load is $P \approx 100$ kW, the EUV power in the 11.2 nm $\pm$ 1% band is 9 kW, and the electron temperature is 63 eV. Variation of the gas puff rate with maintenance of the same total power would result in the red hyperbolalike curve shown in Fig. 3.

In Fig. 4, we show the EUV conversion efficiency and corresponding total power load into electrons as a function of the gas pressure for different nozzle diameters. The conversion efficiency slowly rises with increase of the diameter and saturates at about 15% when the emitting region becomes large enough to switch on the essential trapping of EUV radiation. At the same time, the power required to support the optimal discharge (with the maximal conversion efficiency) increases sharply with

the diameter (see the series of black points in Fig. 4). Thus, the total deposited power determines the optimal nozzle diameter—it should be as wide as possible while being consistent with the available power (see the star in Fig. 4). Such fully optimized conditions may result in undesirably high gas fluxes and plasma densities in a practical design of the EUV light source. In this case, it is possible to reduce the pressure as compared with the optimal pressure and sacrifice EUV efficiency (see the series of red points corresponding to the same power load).

The power deposited into the discharge is ultimately determined by the microwave power delivered from a gyrotron. Most advanced gyrotrons are developed for magnetic-nuclear-fusion research [33,34]. Such devices are able to provide megawatt power in long pulses (up to 1000 s) or cw mode at selected frequencies between 60 and 170 GHz. The cutoff plasma density for the electromagnetic wave at 170 GHz is 3.6×10^{14} cm^{-3}, which is 4 orders of magnitude less than a typical electron density inside the emitting zone of the xenon jet. This is not extremely critical because of the following:

(a) As noted before, the microwave absorption may be shifted toward lower densities in the expanding jet.

(b) For smoothly inhomogeneous plasma droplets that are small compared with the wavelength, effective absorption is possible for much higher densities than the formal cutoff density (strictly defined for a plane wave in infinite medium); see, for example, Ref. [35].

However, there are many reasons for going to higher heating frequencies, among them are the following:

(a) The possibility to focus the microwave beam to a smaller volume.
(b) A large distance between the heating and emitting zones is prone to additional power losses and plasma instabilities.
(c) At nearly atmospheric pressure, microwave breakdown and plasma ramp up at initial stages of the discharge are easier than at higher heating frequencies; for our conditions, this statement has been confirmed experimentally [17,36].

Few high-power gyrotrons operating at frequencies of 250–670 GHz are being developed [18,19,34]. These devices, providing peak power on the order of 100 kW in pulsed mode with the potential of operating in cw mode,
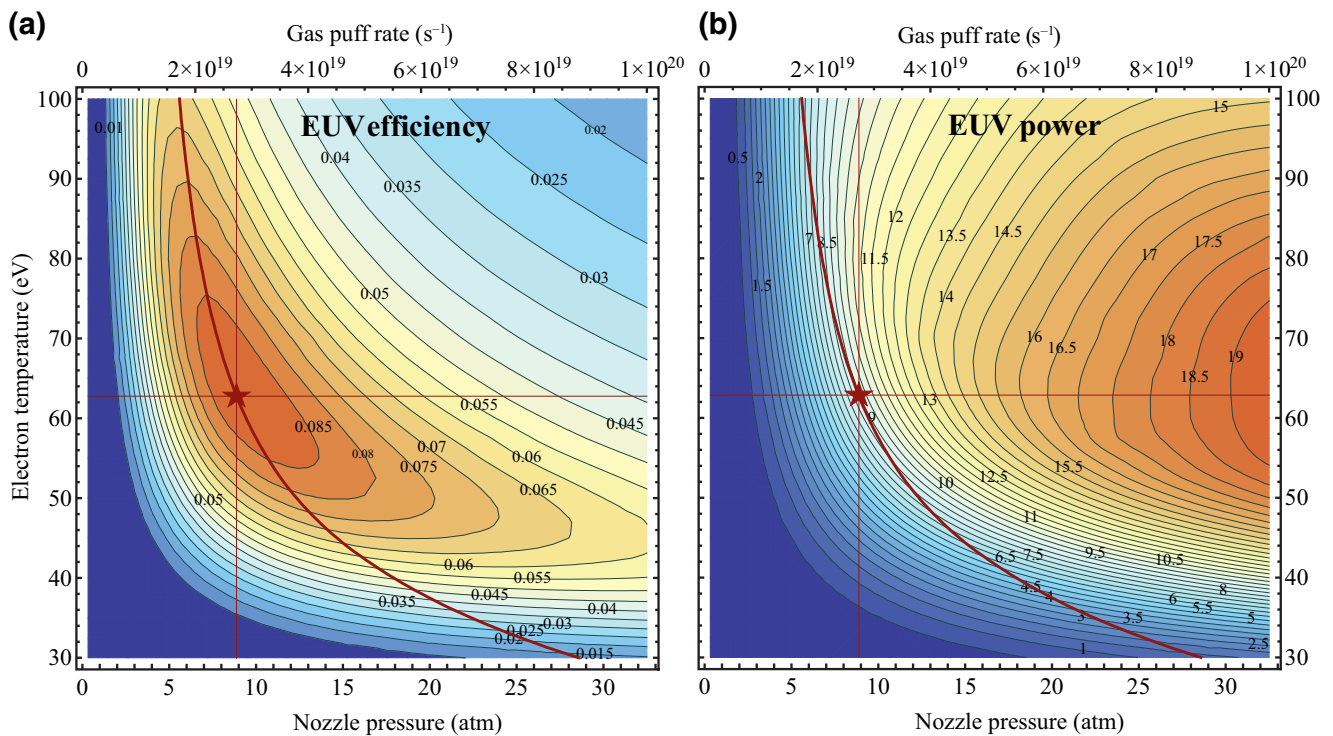

FIG. 3.   EUV conversion efficiency (a) and EUV power (b) for the 11.2 nm $\pm$ 1% band as functions of electron temperature T_e and pressure at the nozzle output p (or, equivalently, gas puff rate F) for constant nozzle diameter $d = 30$ μm, jet divergence $\vartheta = \pi/2$, and nozzle-to-collector distance $L = 5$ cm; ★ indicates the maximum conversion efficiency at $F = 2.7 \times 10^{19}$ s^{-1} and $T_e = 63$ eV; the bold red curve crossing ★ corresponds to constant total power load $P = 100$ kW.

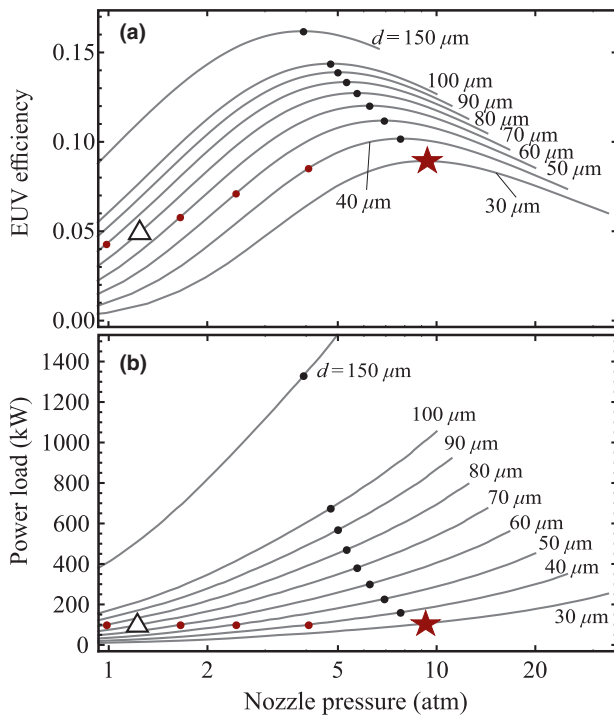FIG. 5. Discharge parameters as a function of coordinate x along the flow (distance from the nozzle output). Top: linear density σp_{EUV} of the power losses in the 11.2 nm $\pm$ 1% spectral region (violet line), plasma flow velocity u (red), and average ion charge $\langle Z \rangle$ (blue). Bottom: electron density n_e (thick line) and densities of ion species n_j (thin lines). The parameters correspond to the point indicated by ★ in Fig. 4.

FIG. 4. EUV conversion efficiency (a) and required total power load P (b) as functions of pressure p at the nozzle output for different nozzle diameters d; ★ and black points indicate the maximum conversion efficiency and red points correspond to fixed power load $P = 100$ kW. The parameters are the same as in Fig. 3.

are likely most suitable for the proposed EUV-source concept.

VI. EXAMPLE OF AN EUV SOURCE WITH A 200-kW, 250-GHZ GYROTRON

The optimal point in Figs. 3 and 4 (indicated by a star) corresponds to a feasible experiment aimed at demonstration of a physical prototype of an EUV light source with a xenon jet, which is in preparation at the Institute of Applied Physics of the Russian Academy of Sciences. The experiment is conducted with a recently developed gyrotron operating at 250 GHz [20]. This tube is designed for cw operation at an output power of 200 kW. Presently it works in pulsed mode (the pulse length is up to 50 μs with a repetition rate 10 Hz) due to limitations of the available power supply. In pulsed mode the gyrotron provides a peak power of up to 330 kW.

Because electrodynamic issues are outside the scope of this paper, we just summarize our present understanding. On the basis of techniques developed in Refs. [35,37], we estimate the maximal fraction of electromagnetic radiation absorbed by the plasma as 10%–50%. The uncertainty depends on the plasma density distribution and overall discharge dimensions (up to few millimeters).
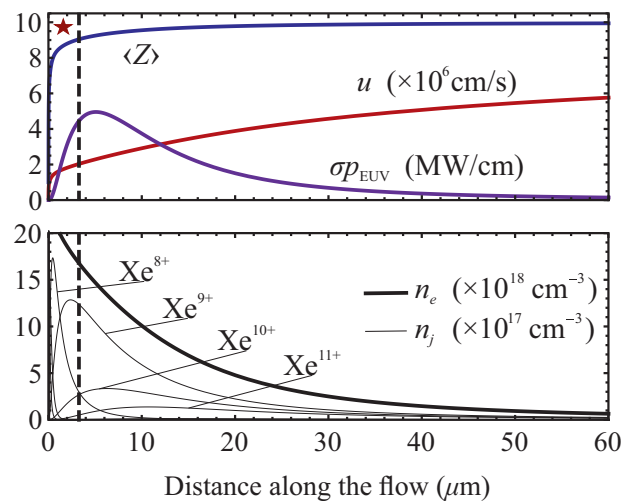
Thus, in the most optimistic case, the power load into the electron component is about 100 kW. This value dictates the optimal nozzle diameter, 30 μm. The maximum EUV conversion efficiency in the 11.2 nm $\pm$ 1% band is 9% (or 4.5% if defined as a fraction of the total microwave power from the gyrotron) is achieved with a puff rate of 2.7×10^{19} s^{-1}. As already mentioned, such a source provides 9 kW of EUV light when operating at an electron temperature of about 60 eV and with cold ions. The expected pressure inside the nozzle is 9 atm, which is acceptable from a technological point of view.

Distributions of discharge parameters along the jet are shown in Fig. 5. The maximum emissivity in the EUV band corresponds to the distance from the nozzle output $x = 5$ μm; this characterizes the linear dimensions of the emitting spot. This point corresponds to the ion-acoustic transition $u = v_a$, which actually is a result of the optimization since after this point the ion charge cannot increase substantially [21]. Inside the EUV emitting zone, the electron density and average ion charge are 1.7×10^{19} cm^{-3} and $\langle Z \rangle = 9$, respectively. The emitting zone repeats the shape of the Xe^{10+} density as this ion has the strongest lines at 11.2 nm $\pm$ 1%. After the sonic barrier, the average ion charge is nearly constant, while all densities fall due to the geometric divergence and further accelerating of the plasma flow. The cutoff plasma density is about 1 mm from the nozzle, which may roughly characterize the largest possible dimension of the microwave-absorption region.

As high initial pressure and subsequent high electron and ion densities may potentially lead to technical difficulties, at least in a proof-of-principle experiment, we
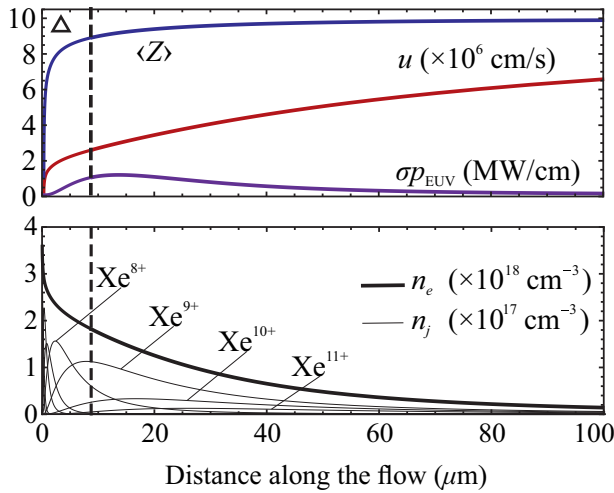
FIG. 6. Same as Fig. 5 except the nozzle diameter $d = 70$ μm. The parameters correspond to the point indicated by $\triangle$ in Fig. 4.
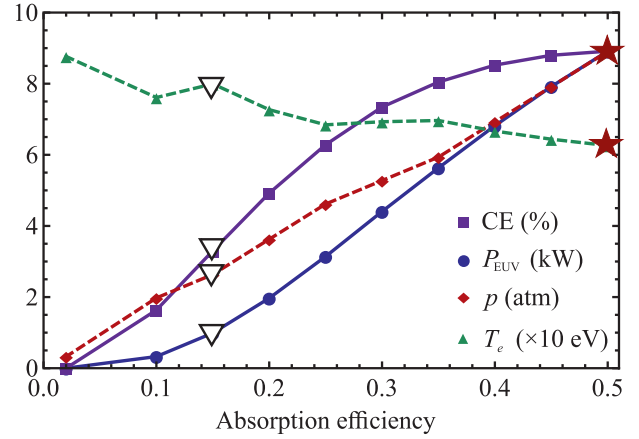

FIG. 7. EUV conversion efficiency (CE), EUV power P_{EUV}, optimal nozzle pressure p, and electron temperature T_e versus microwave-absorption efficiency P/P_0 (defined as the ratio of varied loaded power P to the gyrotron power $P_0 = 200$ kW). The gas puff rate corresponds to maximal EUV power; the other parameters are as in Fig. 3.

also mention the not-optimal case indicated by the triangle in Fig. 4. Here we assume a nozzle twice as wide with diameter 70 μm and keep the same power deposited into the discharge. This change essentially relaxes the conditions for the pressure and density—the pressure inside the nozzle and the electron density reduce to 1.2 atm and 1.8×10^{18} cm^{-3}, respectively. The EUV conversion efficiency also reduces, to 5%, but not drastically. Such a source provides about 5 kW of EUV light when operating at a electron temperature of about 100 eV and gas puff rate $F = 2 \times 10^{19}$ s^{-1}. The spatial distributions of the discharge parameters along the jet are shown in Fig. 6; except for different vertical scales, they are very similar to those shown in Fig. 5.

Finally, we consider the case when the fraction of microwave radiation absorbed by the plasma falls below the optimistic value of 50%. The corresponding degradation of EUV power and efficiency is illustrated if Fig. 7, where the abscissa shows the loaded power as a fraction of injected power provided by the 200-kW gyrotron, the nozzle diameter is 30 μm, and the gas puff is adjusted in a such a way that the EUV power takes the maximal possible value at each point. A decrease of the loaded power leads to an almost-linear decrease of the EUV power. To keep the optimal (for EUV) high ion charge with a reduced power load, one should lower the plasma density by decreasing the gas pressure. One can see that, with a small-enough nozzle, an EUV power of 1 kW, which is still of great interest for applications, is possible with a microwave-absorption efficiency of about 15%; see the inverted triangles in Fig. 7. The characteristics of this regime are as follows: the nozzle pressure is 2.6 atm, the gas puff rate is 8.1×10^{18} s^{-1}, the electron density inside the emitting region is 4.2×10^{18} cm^{-3}, and the electron temperature is 80 eV.

VII. CONCLUSIONS

We consider the concept of an EUV light source based on the line emission of multiply charged xenon ions formed and supported in a plasma jet by microwave radiation of high-power gyrotrons. Theoretical modeling, partially confirmed in preliminary experiments at a density level 2 orders of magnitude lower than discussed here, shows the possibility to obtain EUV conversion efficiencies comparable to or even exceeding the efficiencies of analogous laser-produced plasma devices. Radiation trapping, a new physics aspect considered in the present paper, may affect the energy balance in the dense xenon jet and the EUV conversion efficiency significantly, but this influence is mostly positive as radiation of unwanted lines with low transition energies is trapped in the discharge volume at lower densities than the EUV lines. The physics of formation and supporting of an EUV-radiating plasma jet appears to be clear and robust. In this context, we rely on ongoing experimental verification of theoretical scaling and further fast progress in the development of high-power subterahertz gyrotrons.

Note added after the paper was accepted. Preliminary results of the experiment discussed in Sec. VI are now available; see Ref. [38].

[1] V. Bakshi, *EUV Sources for Lithography* (The Society of Photo-Optical Instrumentation Engineers, Cardiff, 2006).

[2] C. Wagner and N. Harned, EUV lithography: Lithography gets extreme, Nat. Photonics **4**, 24 (2010).

[3] S. S. Andreev, A. D. Akhsakhalyan, M. A. Bibishkin, N. I. Chkhalo, S. V. Gaponov, S. A. Gusev, E. B. Kluenkov, K. A. Prokhorov, N. N. Salashchenko, F. Schafers, and S. Yu. Zuev, Multilayer optics for XUV spectral region: Technology fabrication and applications, Cent. Eur. J. Phys. **1**, 191 (2003).

[4] H. Mizoguchi, H. Nakarai, T. Abe, K. M. Nowak, Y. Kawasuji, H. Tanaka, Yu. Watanabe, T. Hori, T. Kodama, Yu. Shiraishi, T. Yanagida, T. Yamada, T. Yamazaki, S. Okazaki, and T. Saitou, Performance of 250W high power HVM LPP-EUV source, Proc. SPIE **10143**, Extreme Ultraviolet (EUV) Lithography VIII, 101431J (2017).

[5] A. A. Schafgans, D. Brown, I. Fomenkov, R. Sandstrom, A. Ershov, G. Vaschenko, R. Rafac, M. Purvis, S. Rokitski, Ye. Tao, D. Riggs, W. Dunstan, M. Graham, N. Farrar, D. Brandt, N. Bowering, A. Pirati, N. Harned, C. Wagner, H. Meiling, and R. Kool, Performance optimization of MOPA pre-pulse LPP light source, Proc. SPIE **9422**, Extreme Ultraviolet (EUV) Lithography VI, 94220B (2015).

[6] S. K. Moore, EUV lithography finally ready for fabs, IEEE Spectr. **55**, 46 (2018).

[7] A. V. Vodopyanov, S. V. Golubev, D. A. Mansfeld, A. G. Nikolaev, K. P. Savkin, N. N. Salashchenko, N. I. Chkhalo, and G. Yu. Yushkov, Extreme-ultraviolet source based on the electron-cyclotron-resonance discharge, JETP Lett. **88**, 95 (2008).

[8] N. I. Chkhalo, S. V. Golubev, D. Mansfeld, N. N. Salashchenko, L. A. Sjmaenok, and A. V. Vodopyanov, Source for extreme ultraviolet lithography based on plasma sustained by millimeter-wave gyrotron radiation, J. Micro. Nanolithogr. MEMS MOEMS **11**, 021123-1 (2012).

[9] A. V. Vodopyanov, S. V. Golubev, D. A. Mansfeld, N. N. Salashchenko, and N. I. Chkhalo, An extreme ultraviolet radiation source based on plasma heated by millimeter range radiation, Bull. Russ. Acad. Sci.: Phys. **75**, 64 (2011).

[10] S. Churilov, Y. N. Joshi, and J. Reader, High-resolution spectrum of xenon ions at 13.4 nm, Opt. Lett. **28**, 1478 (2003).

[11] S. S. Churilov, Y. N. Joshi, J. Reader, and R. R. Kildiyarova, $4p^64d^8$–$(4d^75p + 4d^74f + 4p^54d^9)$ transitions in Xe XI, Phys. Scr. **70**, 126 (2004).

[12] S. S. Churilov and Y. N. Joshi, Analysis of the $4p^64d^84f$ and $4p^54d^{10}$ configurations of Xe X and some highly excited levels of Xe VIII and Xe IX ions, Phys. Scr. **65**, 40 (2002).

[13] E. B. Saloman, Energy levels and observed spectral lines of xenon, Xe I through Xe LIV, J. Phys. Chem. Ref. Data **33**, 765 (2004).

[14] N. I. Chkhalo and N. N. Salashchenko, Next generation nanolithography based on Ru/Be and Rh/Sr multilayer optics, AIP Adv. **3**, 082130 (2013).

[15] M. Y. Glyavin, S. V. Golubev, I. V. Izotov, A. G. Litvak, A. G. Luchinin, S. V. Razin, A. V. Sidorov, V. A. Skalyga, and A. V. Vodopyanov, A point-like source of extreme ultraviolet radiation based on a discharge in a non-uniform gas flow sustained by powerful gyrotron radiation of terahertz frequency band, Appl. Phys. Lett. **105**, 174101 (2014).

[16] A. V. Vodopyanov, Sources of ultraviolet light based on microwave discharges, EPJ Web Conf. **149**, 02009 (2017).

[17] A. V. Vodopyanov, A. V. Sidorov, S. V. Razin, D. S. Sidorov, A. G. Luchinin, A. P. Fokin, A. I. Tsvetkov, A. P. Veselov, M. Yu. Glyavin, and S. V. Golubev, in *Proceedings of the 42nd International Conference on Infrared, Millimeter, and Terahertz Waves (IRMMW-THz), Cancun, Mexico* (IEEE, Los Alamitos, 2017).

[18] M. Yu. Glyavin, A. G. Luchinin, G. S. Nusinovich, J. Rodgers, D. G. Kashyn, C. A. Romero-Talamas, and R. Pu, A 670 GHz gyrotron with record power and efficiency, Appl. Phys. Lett. **101**, 153503 (2012).

[19] M. Glyavin and G. Denisov, in *Proceedings of the 42nd International Conference on Infrared, Millimeter, and Terahertz Waves (IRMMW-THz), Cancun, Mexico* (IEEE, Los Alamitos, 2017).

[20] G. G. Denisov, M. Yu. Glyavin, A. P. Fokin, A. N. Kuftin, A. I. Tsvetkov, A. S. Sedov, E. A. Soluyanova, M. V. Bakulin, E. V. Sokolov, E. M. Tai, M. V. Morozkin, M. D. Proyavin, and V. E. Zapevalov, First experimental tests of powerful 250 GHz gyrotron for future fusion research and CTS diagnostics, Rev. Sci. Instrum. **89**, 084702 (2018).

[21] A. G. Shalashov, I. S. Abramov, S. V. Golubev, and E. D. Gospodchikov, Theory of a stationary microwave discharge with multiply charged ions in an expanding gas jet, JETP **123**, 219 (2016).

[22] I. S. Abramov, E. D. Gospodchikov, and A. G. Shalashov, Formation of a multi-charged plasma in the directed gas flow, Radiophys. Quantum Electron. **58**, 914 (2016).

[23] A. G. Shalashov, S. V. Golubev, I. S. Abramov, and E. D. Gospodchikov, Formation of UV-radiating strongly non-equilibrium plasma with multiply charged ions in the expanding high-pressure gas jet, AIP Conf. Proc. **1771**, 070001 (2016).

[24] I. S. Abramov, E. D. Gospodchikov, and A. G. Shalashov, Prospects of extreme ultraviolet radiation sources based on microwave discharge for high-resolution lithography, Phys. Plasmas **24**, 073511 (2017).

[25] L. M. Biberman, V. S. Vorob'ev, and I. T. Iakubov, *Kinetics of Nonequilibrium Low-Temperature Plasma* (Nauka, Moscow, 1982).

[26] J. P. Apruzese, An analytic Voigt profile escape probability approximation, J. Quant. Spectrosc. Radiat. Transfer **34**, 447 (1985).

[27] J. D. Huba, NRL Plasma Formulary Report No. NRL/PU/6790–04-477, 2004. Equation (4) on p. 53.

[28] R. D. Cowan, *The Theory of Atomic Structure and Spectra* (University of California Press, Berkeley, 1981).

[29] H. Van Regemorter, Rate of collisional excitation in stellar atmospheres, Astrophys. J. **136**, 906 (1962).

[30] D. H. Sampson and H. L. Zhang, Use of the Van Regemorter formula for collision strengths or cross-sections, Phys. Rev. A **45**, 1556 (1992).

[31] Y. Izawa, K. Nishihara, H. Tanuma, A. Sasaki, M. Murakami, A. Sunahara, H. Nishimura, S. Fujioka, T. Aota, Y. Shimada, M. Yamaura, M. Nakatsuka, H. Fujita, K. Tsubakimoto, H. Yoshida, N. Miyanaga, and K. Mima, EUV light source by high power laser, J. Phys.: Conf. Ser. **112**, 042047 (2008).

[32] V. M. Povyshev, A. A. Sadovoy, V. P. Shevelko, G. D. Shirkov, E. G. Vasina, and V. V. Vatulin, Electron-impact

ionization cross sections of H, He, N, O, Ar, Xe, Au, Pb atoms and their ions in the electron energy range from threshold up to 200 keV, JINR Commun. No. E9-2001-148, 2001, http://www1.jinr.ru/Preprints/2001/e9-2001-148.pdf.

[33] G. G. Denisov, A. G. Litvak, V. E. Myasnikov, E. M. Tai, and V. E. Zapevalov, Development in Russia of high-power gyrotrons for fusion, Nucl. Fusion **48**, 054007 (2008).

[34] M. Thumm, State-of-the-art of high power gyro-devices and free electron masers, Karlsruhe Institute of Technology Report No. KIT-SR 7735, 2016 (DOI:10.5445/KSP/10000 68193).

[35] A. Shalashov and E. Gospodchikov, Simple approach to electromagnetic scattering by small radially inhomogeneous spheres, IEEE Trans. Antennas Propag. **64**, 3960 (2016).; On the determination of the electromagnetic field upon scattering by a small inhomogeneous spherical object, JETP **123**, 587 (2016).

[36] A. V. Sidorov, S. V. Razin, A. G. Luchinin, A. I. Tsvetkov, A. P. Fokin, D. S. Sidorov, A. P. Veselov, A. V. Vodopyanov, and M. Y. Glyavin, Gas breakdown by a focused beam of THz waves, EPJ Web Conf. **149**, 02031 (2017).

[37] A. G. Shalashov, S. V. Golubev, E. D. Gospodchikov, and A. V. Vodopyanov, in *Strong Microwaves and Terahertz Waves: Sources and Applications, Proceedings of the 8th International Workshop, Nizhny Novgorod, July 9–16, 2011*, edited by A. G. Litvak (Institute of Applied Physics RAS, Nizhny Novgorod, 2011), p. 194.

[38] A. G. Shalashov, A. V. Vodopyanov, I. S. Abramov, A. V. Sidorov, E. D. Gospodchikov, S. V. Razin, N. I. Chkhalo, N. N. Salashchenko, M. Yu. Glyavin, and S. V. Golubev, Observation of extreme-ultraviolet light emission from an expanding plasma jet with multiply-charged argon or xenon ions, arXiv:1807.06836 [physics.plasm-ph]; Appl. Phys. Lett. (DOI: 10.1063/1.5049126, to be published).